

The PANDA automatic weather station network ~~-~~ between the coast and Dome A, East Antarctica

Minghu Ding¹, Xiaowei Zou^{1,2}, Qizhen Sun³, Diyi Yang¹, Wenqian Zhang¹, Lingen
Bian¹, Changgui Lu¹, Ian Allison⁴, Petra Heil^{5,4}, Cunde Xiao^{6,5}

¹State Key Laboratory of Severe Weather, Chinese Academy of Meteorological
Sciences, Beijing 100081, China

²GNSS research center, Wuhan University, Wuhan 430079, China

³Polar Research and Forecasting Division, National Marine Environmental
Forecasting Center, Beijing 100081, China

⁴[Institute for Marine and Antarctic Studies, University of Tasmania, Australia](#)

^{5,4}Australian Antarctic Division and Australian Antarctic Program Partnership,
University of Tasmania, Australia

^{6,5}State Key Laboratory of Earth Surface Processes and Resource Ecology, Beijing
Normal University, Beijing 100875, China

Correspondence to: Minghu Ding (dingminghu@foxmail.com) and Cunde Xiao
(cdxiao@bnu.edu.cn)

Abstract: This paper introduces a unique multiyear dataset and the monitoring capability of the PANDA automatic weather station network which includes eleven automatic weather stations (AWS) across Prydz Bay-Amery Ice Shelf-D~~e~~ome A area from the coast to the summit of the East Antarctica ice sheet. The ~1460 km transect from Zhongshan to Panda S ~~station~~ follows roughly along ~77° E longitude and covers all geographic ~~and climatic~~ units of East Antarctica. Initial inland observations, near the coast, started in the 1996/1997 austral summer. All AWSs in this network measure air temperature, relative humidity, air pressure, wind speed and wind direction at 1-hour intervals, and some of them can also measure firn temperature and shortwave/longwave radiation. Data are relayed in near real-time via the ARGOS system. Data quality is generally very reliable and the data have been used widely. In this paper, we firstly present a detailed overview of the AWSs, including the sensor characteristics, installation procedure, data quality control protocol, and the basic analysis of each variable. We then give an example of a short-term atmospheric event that shows the monitoring capacity of the PANDA AWS network. This dataset, which is publicly available, is planned to be updated on a near-real time and should be valuable for climate change estimation, extreme weather events diagnosis, data assimilation,

34 weather forecasting, etc. The dataset is available at
35 <https://doi.org/10.11888/Atmos.tpcd.272721> (Ding et al., 2022).

36 **1. Introduction**

37 Antarctica, covered by a vast ice sheet, has the coldest climate on Earth's surface
38 (Qin and Ren, 2001; Van den Broeke and Van Lipzig, 2003; Zhou et al., 2009). Great
39 efforts have been made to study Antarctic climate change under global warming
40 because of its role in the climate system and its ~~capability~~~~capacity~~ to greatly impact
41 global sea level rise (IPCC, 2019; Huai et al., 2019). However, the reliability of
42 Antarctic climate change estimation and weather forecasting is still under debate (Hines
43 et al., 2019; Zhang et al., 2021). This is a consequence of the paucity of observations,
44 especially at long term inland weather stations, which can be directly assimilated in to
45 models and reanalysis data (Vignon et al., 2017; Wei et al., 2019).

46 The first attempt at automatic weather station (AWS) observations in Antarctica was
47 in 1956/57, when station XG1 was deployed by the United States near McMurdo; but
48 this station was short lived (Lazzara et al., 2012). Early attempts at AWS observations
49 were also made off the coast of East Antarctica by the Australian National Antarctic
50 Research Expedition (ANARE) at Chick Island (in 1961) and Lewis Island (in 1962).
51 Both these stations were also short lived.

52 Development of automatic observational technology in polar regions was greatly
53 advanced with initiation, in 1978, of the ARGOS data relay system on polar orbiting
54 satellites. This, together with more robust and power-efficient electronics, saw
55 successful Antarctic AWS deployments by the University of Wisconsin, USA,
56 commencing in 1980. The Australian Antarctic Division ([AAD](#)) also tested its design
57 of AWS at near-coastal sites in 1980 and deployed its first successful station on the
58 inland ice sheet, at 1830 m elevation, in January 1982 (Allison and Morrissey, 1983).
59 Subsequently, more and more Antarctic AWSs were installed: ~30 by 1990, ~55 by
60 2000, ~60 by 2010 and ~160 by 2020 (Bromwich et al., 2020). Many of these were
61 installed as part of a United States network on the Ross Ice Shelf, inland from the Adélie
62 Land coast for a study of katabatic wind flow, and at other interior ice sheet sites
63 (Lazzara et al., 2012). During the International Antarctic Glaciological Project traverses
64 from Casey station, ~~a number~~ of ANARE AWSs were deployed on the ice sheet, along
65 about 110°E to 3096 m elevation. Australian glaciological traverses between Mawson
66 and Zhong-Shan ~~stations~~ deployed 5 AWSs at 2500 m elevation around the interior of

67 the Lambert Glacier Basin (LGB), between 1990 and 1994 (Allison et al., 1993;
68 Allison, 1998; Heil, 2006). Further west in eastern Dronning Maud Land, stations were
69 built and deployed on the ice sheet by Japan at Dome Fuji (in December 1993) and
70 Relay (in January 1993) (Enomoto et al., 1995). To extend knowledge of the near-
71 surface climate and heat budget of Antarctica, Netherlands started to deploy AWSs in
72 western Dronning Maud Land in January 1997 (Reijmer and Oerlemans, 2002).

73 Several of the AWSs mentioned failed after a relatively short time, and those in high
74 accumulation near-coastal areas became buried by snow. But quite a few continued to
75 provide high-quality data for many years. For example, the Australian AWS at GC41,
76 inland of Casey at 2760 m elevation, provided good data for more than 21 years until
77 eventually buried, although it was never visited for maintenance. The interior ice sheet
78 with low accumulation, relatively low wind speeds, and no liquid water is ~~actually a~~
79 benign environment for electronic systems if properly designed for very low
80 temperatures. The higher latitude sites also see more transits of polar-orbiting satellites
81 carrying the ARGOS data relay system.

82 These AWS observations have made valuable contributions to Antarctic research.
83 Firstly, the data have been used to evaluate weather and climate changes (Turner et al.,
84 2005; 2007; Wei et al., 2019; Wang et al., 2022). For example, Schwerdtfeger (1984)
85 gave a brief characterization of the inland Antarctica climate from AWS data. Allison
86 et al (1993) analyzed the influence of ice sheet topography on surface meteorology
87 using 10 AWSs from both the US-French network in Adélie Land and the Australian
88 network inland of Casey. Secondly, AWS data, including radiation measurements, can
89 be used to investigate ice/snow-atmosphere interaction processes in Antarctica. Van den
90 Broeke et al. (2004a; 2004b; 2005; 2006) studied the daily and seasonal variation of the
91 surface energy balance in detail in Dronning Maud Land. Ding et al. (2020; 2021a)
92 improved the surface energy balance simulation scheme at Dome A and the inland
93 Antarctic area with long term AWS measurements. Thirdly, AWS observations are also
94 critical in evaluating the applicability of reanalysis data and numerical models in
95 Antarctica. Nigro et al. (2011) estimated the performance of Antarctic Mesoscale
96 Prediction System (AMPS) under varied synoptic conditions with AWS data for the
97 Ross Ice Shelf. Xie et al (2014) assessed the accuracy of daily mean surface pressure
98 from different meteorological reanalyzes against in situ observations from automatic
99 weather stations in East Antarctica. Dong et al. (2020) evaluated the robustness of near-
100 surface wind speed of multiple global atmospheric reanalysis in Antarctica based on

101 many AWS and meteorological observations made at staffed stations. Recently, Wei et
102 al. (2019) and Turner et al. (2020) used multiple meteorological records to give the
103 spatial/temporal distribution of temperature extremes across Antarctica for the first time.

104 However, most staffed observational sites and AWSs in Antarctica are still mainly
105 located in the coastal area, and data from the sparse inland sites is interrupted frequently
106 (e.g., the anemometer was often frozen during austral winter at Eagle, ~~and~~ Dome A)
107 (Wendler et al., 1988; Van As et al., 2005; Zhou et al., 2009; Lazzara et al., 2012; Sun
108 et al., 2018; Bromwich et al., 2020). More continuous and systematic AWS observation,
109 are still required from Antarctica.

110 Commencing in [the](#) 1996/1997 austral summer, the Chinese National Antarctic
111 Research Expedition (CHINARE) started deploying AWSs between the coastal
112 Zhongshan and inland Panda S (the PANDA transect). The first stations ~~was~~ deployed
113 on this transect were manufactured by the ~~Australian Antarctic Division~~ AAD, but after
114 2012, the Chinese Academy of Meteorological Sciences made great progress in AWS
115 design, especially the ultra-low temperature power supply system (patent for invention,
116 Ding et al., 2021b), and deployed 7 further AWSs along the PANDA transect.

117 Initial studies using these observations focused on the coastal area or a single site
118 (e.g., van den Broeke et al., 2004a; 2004b; Chen et al., 2010) while later studies used
119 data from more inland stations (Ma et al., 2010; Ding et al., 2021a). Only a few studies
120 have used meteorological information (~~shown in Table. 1~~) from the whole transect
121 (Zhou et al. 2009; Ma et al. 2010; Bian et al. 2016). That is because only 5 of the initial
122 AWSs ~~were still operating~~ ~~survived till in~~ 2012 (~~include Dome A, Eagle, and Panda~~
123 ~~N, Zhongshan and Panda S~~), others ~~had~~ ~~ve~~ been buried by snow accumulation or ~~stop~~
124 ~~operation failed~~ due to low air temperature (Ding et al., 2021a). ~~and~~ ~~s~~ Subsequently
125 ~~AWSs have been installed close to their~~ ~~locations of the failed stations to extend the~~
126 ~~measurements (e.g., Panda 200 was installed close to LGB69).~~ ~~These were Dome A,~~
127 ~~Eagle, and Panda N (Australian Antarctic Division), Zhongshan and Panda S (Chinese~~
128 ~~Academy of Meteorological Sciences).~~ The more recent deployments now provide ~~a~~
129 consistent, high quality and real time meteorological observations from the PANDA
130 AWS network. Some data from the PANDA AWS network have been compiled by
131 WMO (e.g., Dome A ID: 89577, Eagle ID: 89578, Kunlun ID: 89572, Taishan ID:
132 89576) and some are available as monthly means from the Scientific Committee on
133 Antarctic Research (SCAR) Reference Antarctic Data for Environmental Research
134 (READER)

(<https://www.bas.ac.uk/project/reader/http://www.antarctica.ac.uk/met/READER/>).

But most of these data have not been published before. Here, ~~in order to~~ promote and make available the value of these AWSs data, we provide metadata of the dataset that will be updated ~~on a~~ near-real time ~~in A~~ on the platform “Big Earth Data Platform for Three Poles” (<http://poles.tpdc.ac.cn/zh-hans/>). We also provide an overview of the climate characteristics of the ~~site~~ region.

2 Observation region and data ~~pre~~-processing

2.1 Observation region and site descriptions

The PANDA transect is approximately along 77° E longitude, and stretches approximately 1460 km from the coast at Zhongshan to the ~~dome region at~~ Dome A, ~~region at~~ the summit of the East Antarctic Ice Sheet. This transect is highly representative of East Antarctica—~~highly~~, for it covers Prydz Bay, Lambert Glacier/Amery Ice Shelf, high inland and dome ~~summit~~ regions. According to Zhang et al. (2008) and Ding et al. (2011), the PANDA transect can be divided into three typical topographies: a coastal region characterized by steep terrain (corresponding to Zhongshan to Panda 200), an inland region with strong katabatic wind (Panda 300 to Eagle), and a dome region (Panda 1100 to Panda S). ~~The PANDA transect includes almost all the climate types in East Antarctica.~~

The PANDA AWS network had 11 AWSs in operation in 2022: Zhongshan, Panda 100, Panda 200 (LGB 69), Panda 300, Panda 400, Taishan, Eagle, Panda 1100, Dome A, Kunlun and Panda S. All of them are located on the western side of the ~~Lambert Glacier Basin~~ LGB (Fig. 1), at different latitudes (69° S-83° S) and at different elevations (detailed information can be found in Table 1). The first site, Zhongshan was established in March 1989, when CHINARE first arrived in East Antarctica (~~Zeng et al., 2021~~). It was initially a Staffed Weather Station but has now ~~has been~~ replaced by an AWS. LGB 69 (192 km from the coast) was first deployed in January 2002 during the ~~AAD Lambert Glacier Basin~~ traverse. ~~This station was in a region of high ice velocity (17.7 m a⁻¹) and high accumulation rate (199 kg m⁻² a⁻¹ for 2002-2003) (Zhang et al., 2008; Ma et al., 2010; Ding et al., 2011; 2015) and it became buried approximately every 3 years, requiring digging up and redeploying on the surface. It stopped operating by 2008 (Ding et al., 2021a). Since it was difficult to maintain an AWS at the original site, PANDA 200 was deployed 200 km from the coast in December 2016, and is considered as a replacement AWS for LGB 69.~~ In January 2005, Eagle and

168 Dome A were installed during the CHINARE 21th which reached the summit of East
169 Antarctic Ice Sheet, ~1248 km from the coast, ~~the observed lowest air temperature~~
170 ~~was 80.36 °C (0300 UTC, 3 September 2007) at height of 4 m on Dome A.~~ Then in
171 January 2008, Panda S was deployed in cooperation with the University of Wisconsin
172 as a contribution to the International Polar Year, but this AWS has ~~been only operated~~
173 ~~intermittently~~intermittent. The other AWSs ~~were deployed during 2012 and 2019, and~~
174 were manufactured by the Chinese Academy of Meteorological Sciences ~~and were~~
175 ~~deployed during 2012 (Taishan) and 2019 (Panda 100, Panda 300, Panda 400).~~ The
176 hourly data from the all AWSs are remotely collected and relayed in near real-time ~~only~~
177 by the ARGOS System ~~and not saved internally.~~ ~~The data is not stored internally.~~

178 It should be noted that these AWSs are of several different designs for different
179 scientific purposes. All include sensors for air temperature (T_a) and wind speed (WS),
180 initially at 1, 2, 4 and/or 6 m ~~height~~above surface ~~(the surface height and station tilt are~~
181 ~~not part of the monitored variables, all sensors height in this paper is initial height from~~
182 ~~build stations),~~ and wind direction (WD), relative humidity (RH) and air pressure (P).
183 ~~Sensor height above the surface and station tilt are not part of the monitored variables,~~
184 ~~and all sensor heights in this paper are the heights at initial deployment.~~ Panda 300,
185 Taishan, Eagle and Dome A AWSs are also equipped with surface and firn temperature
186 probes (detailed information can be found in Table 1). The Zhongshan is designed to
187 WMO service regulation so the initial height of wind measurement is 10 m.

188 ~~The Chinese Academy of Meteorological Sciences designed AWSs use a HMP155~~
189 ~~resistance probe to measure air temperature and relative humidity; Panda S and which~~
190 ~~uses a Weed PRT 2-wire bridge and Vaisala HMP35A; and Eagle and Dome A use~~
191 ~~FS23D thermistors and HMP35D humidity probe (Xiao et al., 2008).~~ ~~The AWSs that~~
192 ~~were designed by the Chinese Academy of Meteorological Sciences use a Vaisala~~
193 ~~HMP155 resistance probe to measure air temperature and relative humidity. Panda S~~
194 ~~use a Weed wire bridge and Vaisala HMP35A. Eagle and Dome A AWSs use FS23D~~
195 ~~thermistors and HMP35D humidity probes (Xiao et al., 2008). The Vaisala HMP15 is~~
196 ~~an integrated air temperature and relative humidity sensor is an integrated sensor, which~~
197 ~~itself considers the conversion of ice and water form and automatically accounts for~~
198 ~~whether RH is relative to water or ice. The air pressure is single-layer at most stations~~
199 ~~(except Panda 300). The air pressure of sensor for Eagle and Dome A is measured by a~~
200 ~~Paroscientific 6015A. Panda 100 and Taishan use Vaisala PTB110 and Zhongshan uses~~
201 ~~Campbell Scientific CS106 to measure air pressure. A Paroscientific Model 215A~~

202 ~~pressure sensor is mounted to monitor air pressure used at Panda S. The~~ and all other
203 ~~AWS stations use Vaisala PTB210. The~~ Eagle and Dome A ~~AWSs~~ have cup
204 anemometers which ~~stall-freeze~~ during extreme austral winter cold (Zhou et al., 2009;
205 Ma et al., 2010). ~~But~~ the other AWSs are equipped with ~~Huayun Zhongyi~~ XFY3-1
206 wind propeller anemometers and ~~some of them~~ are optimized to prevent “diamond
207 dust” ~~“accumulation on the instruments.~~ ~~Some stations (Panda 100, Panda 200, Panda~~
208 ~~300, Panda 400, Taishan, Panda 1100, Kunlun) also make radiation measurements.~~
209 ~~These are not discussed in this paper, but are available detailed and available for~~
210 ~~download from the data site. Further~~ ~~D~~ details of the sensor and AWS schemes can be
211 found in Table 1.

212 All sensors are calibrated before ~~the AWS deployment~~ ~~fieldwork~~, but ~~extremely super~~
213 cold weather below -60 °C may bring uncertainty. The height of the sensors above
214 surface gradually decreases with snow accumulation, ~~except for Zhongshan which is~~
215 ~~on rock~~. This has been ignored in the preliminary analysis presented here.

216 2.2 Data quality control

217 All data are checked initially to ensure integrity, consistent with the approach of Ma
218 et al. (2010), Lazzara et al. (2012), and Wawrzyniak and Osuch (2020). ~~SA schematic~~
219 ~~diagram of data processing workflow was~~ ~~shown in Figure 2.~~ Firstly, ARGOS
220 reception may lead to duplicated records, ~~or~~ time dislocation (~~Fig. 2~~) ~~and~~, these are
221 removed. For those AWSs with measurements of air temperature and wind ~~speed~~ at
222 multiple levels, a check of the vertical profiles is a particularly strong validation. If the
223 vertical ~~profiles-gradients~~ are ~~near logarithmic~~ ~~physically consistent~~, then the absolute
224 values are ~~sure~~ ~~likely~~ to be accurate. Secondly, different variables are compared to
225 check their consistency. For instance, wind direction will be eliminated when wind
226 speed is zero. In addition, the height of sensors might change with snow
227 accumulation ~~ng~~. ~~The~~ ~~A~~ correction method ~~to~~ ~~for~~ this error ~~have~~ ~~has~~ been introduced in
228 Ma et al. (2008) and Smeets et al. (2018). ~~In addition, the logger box was buried in the~~
229 ~~snow at installation, which has the advantage of not interfering with the radiation~~
230 ~~measurement.~~ Daily mean values are averaged from hourly data and then monthly and
231 annual mean values are progressively calculated. Similarly to the methodology of
232 Maturilli et al. (2013) and Zou et al. (2021), missing values are handled depending on
233 their duration. If more than 21% data (5 hours) during one day, or 12% data (4 days)
234 within one month, or 25% data (3 months) within one year are missing, ~~the~~ ~~this~~

235 daily/monthly/annual data is considered a missing value.

236 The measurements at Zhongshan were made only four times a day (00:00, 06:00,
237 12:00 and 18:00, UTC) from 1 March 1989 to 31 January 2002. Hence, we analyzed
238 diurnal data only from 2002 to 2020 ~~for consistency~~, but monthly ~~and~~ annual ~~data~~
239 values from 1989 to 2020. The average of meteorological variables at other AWSs were
240 calculated for different spans-periods depending on their deployment dates, which are
241 not the same (Table 1): Panda100, Panda 300, Panda 400 and Panda 1100 span from
242 2019 to 2021; Panda 200 spans from 2016 to 2021; Taishan spans from 2012 to 2021;
243 Eagle and Dome A span from 2005 to 2020; Kunlun spans from 2017 to 2021; Panda S
244 spans from 2008 to 2021. All variables are analyzed at a height of 4 m, except at
245 Zhongshan, Panda 200 and Panda 400. The wind speed and direction at Zhongshan are
246 at 10 m ~~height~~, and the air temperature and relative humidity at Panda 200 and Panda
247 1100 are at 6 m and 2 m ~~heights~~, respectively.

248 Due to heavy hoar frost in the Antarctic inland, the anemometers with a vertical axis
249 at Eagle, Dome A and Panda S ~~was~~ often frozen during austral winter ~~at Eagle, Dome~~
250 ~~A and Panda S~~, which ~~may leads~~ to invalid measurements (Zhou et al., 2009). We used
251 a different type of anemometer on the other AWSs and deleted the wintertime wind
252 speed and direction data for ~~those-these~~ three AWSs.

253 3 Results

254 3.1 Air temperature

255 The Mmean diurnal variation of air temperature is ~~obviously an~~ approximately
256 sinusoidal curve at all AWSs (Fig. 3). The maximum air temperature occurs at 0900-
257 1100 UTC (1400-1600, Local StandardSolar Time LST), and the minimum was at
258 2200-2300 UTC (0300-0400, LST). From the coast to the dome area, the standard
259 deviation of diurnal variations gradually increases (from 0.64 °C at Zhongshan to
260 1.42 °C at Panda S), consistent with the result of King et al. (2006). This regularity
261 may be the result of katabatic wind, marine effect and cloud (van den Broeke, et al.,
262 2004a; Zhou et al., 2008).

263 The monthly mean air temperatures ~~at~~, particularly for the more southern AWSs,
264 show a “coreless” winter with a single “valley” pattern; in other words, there is no
265 distinctive minimamimum during austral winter (Fig. 4) (Allison et al., 1993; Chen
266 et al., 2010; Ma et al., 2010). The variability (standard deviation of monthly air
267 temperature) in austral winter is much larger than in austral summer, e.g., 2.46 °C vs

268 1.67 °C at Taishan. This indicates that the Antarctica Ice Sheet experiences more
269 weather activities during austral winter. For example, sometime cyclones from the
270 surrounding ocean may bring warm, moist air masses (Qin et al., 2017; Ding et al.,
271 2020). In addition, the inland region exhibits more dynamic weather ~~either~~ than either
272 the coast or the dome summit regions, coinciding with a larger standard deviation in
273 monthly air temperature. This is 1.5 times (3.24 °C) that of the others two regions
274 (2.19 °C, and 2.39 °C respectively).

275 With consideration of the length of the observation period, the trend in annual mean
276 air temperatures is shown for only 4 AWSs in Fig. 5. These are Zhongshan (1989 to
277 2020), Taishan, (2013 to 2020), Eagle (2005 to 2020) and Dome A (2005 to 2020). They
278 have annual means of -10.0 °C, -35.4 °C, -41.2 °C and -50.4 °C respectively, ~~similar~~
279 ~~to~~like the results of Ma et al. (2010). This difference can be attributed to differences in
280 elevation/topography and latitude (Allison et al., 1993). ~~The annual variations of air~~
281 ~~temperature at the four sites are multivariate. There has been a warming trend at~~
282 ~~Zhongshan of 0.10 °C/decade, and significant increase of air temperature at Taishan of~~
283 ~~1.07 °C/decade. However, there has been no significant change at Eagle (-~~
284 ~~0.13 °C/decade) or Dome A (-0.07 °C/decade), unlike that at Vostok and South Pole~~
285 ~~which are experiencing warming (Clem et al., 2020).~~

286 3.2 Relative humidity

287 The variation of local atmospheric moisture is driven by a combination of large-scale
288 advection and local evaporation/sublimation effects (Maturilli et al., 2013). Figure 6
289 shows a similar distribution to a previous study (Ma et al., 2010); the austral summer is
290 more humid than the austral winter at all AWSs. However, coastal relative humidity
291 fluctuates largely on the monthly scale but there is a little difference between austral
292 summer and winter. At the inland and dome summit regions, the monthly relative
293 humidity has a very clear seasonal cycle (except Dome A).

294 Figure 7 shows the annual averages and trends of relative humidity at Zhongshan,
295 Taishan, Eagle and Dome A. Relative humidity varied considerably at all sites, with the
296 driest records at Dome A. Interestingly, the relative humidity is well correlated with air
297 temperature except at Zhongshan, partially because its weather is controlled by the
298 adjacent ocean.

299 3.3 Air Pressure

300 Air pressure obviously decreases with elevation from coast to dome area, and the
301 seasonal cycles ~~s-also~~ becomes clearer. Monthly mean air pressure shows a semi-annual
302 oscillation with equinoctial minima near the coastal and inland areas along the PANDA
303 AWS network, but is much less distinct at the dome area, ~~this~~. The semi-annual
304 oscillation there could be ~~submerged~~ hidden under larger annual oscillation (Fig. 8)
305 (Radok et al., 1996). Coastal areas like Zhongshan, Panda 100 and Panda 200 have little
306 air pressure difference between austral summer and winter, but there are obvious
307 differences for the inland area, with a stable-strong low-pressure structure at the plateau
308 surface in austral winter. However, there ~~are-is~~ more ~~eyelone-cyclonic activities-activity~~
309 in the inland area (Panda 300 to Eagle) (Ding et al., 2020), ~~showed~~ This is shown by
310 the highest standard deviation of air pressure, (705 ± 4 hPa), higher than the coastal
311 (858 ± 3.10 hPa) and the dome areas (585 ± 2.74 hPa). The annual averages (Table 2)
312 and trend of air pressure at the AWS shows no systematic variation, consistent with
313 Zhou et al. (2009) and most ~~of the~~ other studies in East Antarctica.

314 3.4 Wind speed and direction

315 Diurnal variation in wind speed shows most clearly in the coastal katabatic region
316 (Fig. 9). The maximum wind speed occurs around 0400-0800 UTC (0900-1300 LST)
317 and the minimum around 1400-1600 UTC (1900-2100 LST at near-coastal AWSs.
318 Diurnal variation of wind speed gradually decreases from the coast to the dome region,
319 from Panda 1100 to Panda S, ~~which~~, Panda S showed very weak fluctuation because
320 the dome area is a sink center for atmosphere circulation and the origin of Antarctic
321 surface wind flow (Parish and Bromwich, 1987; Van den Broeke and Van Lipzig, 2003;
322 Aristidi et al., 2005; Das et al., 2013). This phenomenon is also reflected in the vertical
323 temperature gradient difference. At all times of day, the surface atmosphere has a
324 positive temperature gradient (the 4 m air temperature is higher than 2 m). Thus, the
325 wind is ~~stable and~~ weak and wind direction is stable at Dome A. Similarly, Zhou et al.
326 (2009) and Bian et al. (2016) also found that there was a persistent and stable inversion
327 layer due to strong surface cooling of the Antarctic ~~ice-Ice sheet~~ Sheet.

328 There is evidence of seasonal variations of wind speed at ~~most all~~ AWSs except Eagle,
329 Dome A and Panda S. The austral winter wind speed is higher than austral summer (Fig.
330 10). This is related to the intensity of surface cooling and topography of the ice sheet.

331 Wind flow can be accelerated by cooling along a slope (Van den Broeke et al., 2002).
332 The fluctuation of wind speed was much greater in austral winter than in summer, e.g.,
333 the standard deviations at Panda 200 in austral winter and summer were 1.43 m s^{-1} and
334 0.99 m s^{-1} ~~in austral winter and summer~~ respectively. From the coast to dome area, the
335 wind speed ~~became weaker~~decreased, which has also been discussed by Ma and Bian
336 (2014) and can be attributed to the katabatic wind effect. Zhongshan is an exception,
337 its wind speed is weaker than at the other coastal AWSs. This AWS was deployed on
338 rock ~~at the edge of Antarctica~~more than 2 km from the edge of the ice sheet ~~whose~~
339 where the katabatic wind ~~effect was~~ is ~~has~~ weakened. ~~This pattern is also coincidence~~
340 ~~with aerodynamic roughness length, momentum transfer coefficient and friction~~
341 ~~velocity~~ (Van den Broeke et al., 2002; Zhou et al., 2009, Ma et al., 2010).

342 ~~In~~Over the long-term, the wind speed showed a weakening trend over the whole
343 transect (Fig. 11). The trend at Zhongshan was $-0.41 \text{ m s}^{-1}/\text{decade}$ ($p < 0.01$) from 1989
344 to 2020, ~~and there was also a decrease at Taishan ($-0.08 \text{ m s}^{-1}/\text{decade}$) from 2013 to~~
345 ~~2020~~. This phenomenon deserves future investigation.

346 As has been previously noted, the vertical axis anemometers of Dome A and Eagle
347 are often frozen during austral winter, and the data quality of wind during austral fall is
348 poor. Therefore, we ~~only analyzed~~analyzed wind direction ~~in only the half year for the~~
349 ~~months from~~ (September to February) at these two sites. Figure 1 showed the wind
350 rose distribution of all AWSs. The wind directions at coastal and inland areas (from
351 Zhongshan to Taishan) were relatively ~~stable~~regular: during austral summer, constant
352 easterlies determine the wind speed on the ice sheet ~~surface wind, which is thus mainly~~
353 ~~from NE to SE~~. In austral winter, katabatic forcing from strong surface cooling, large-
354 scale pressure gradient and Coriolis force, dominates, ~~it also~~ resulting in winds showed
355 from NE to SE (Van den Broeke et al., 2002; Van den Broeke and Van Lipzig, 2003).
356 At the dome summit region, the wind direction has a broad distribution with weak wind
357 speed south, southeast and west. ~~Especially at the~~At Dome A, ~~no prevailing wind has~~
358 ~~showed from ~18 years observation~~16 years of observations result in ~~show no prevailing~~
359 wind direction.

360 4. Capability of monitoring short-term atmospheric events

361 Compared to other meteorological observations, one advantage of the PANDA AWS
362 network is that it covers all terrain and climatic sectors of East Antarctica. The local
363 weather conditions can be ~~deduced~~reflected from the meteorological surface

364 measurements. Figure 12 shows the course of air pressure, air temperature, relative
365 humidity and wind speed ~~on~~ from 30th July ~~to~~ 3rd August 2020, which indicates the
366 ~~occured~~ occurrence of a prominent blocking event. To assess the capability to monitor
367 weather conditions, this physical atmospheric process was ~~analyzed~~ analyzed by using
368 the PANDA AWSs network dataset.

369 On 1st August 2020, the blocking stretched southward to around 100° E, forming a
370 high-pressure ridge in the interior of ice sheet (~~not shown~~ Fig. 13). The deep low-
371 pressure system was blocked from moving eastward and thus stagnated near Prydz Bay.
372 This situation facilitated the meridional advection of warm, moist air masses. It can be
373 seen in Fig. 12, that the air temperature, relative humidity, air pressure and wind speed
374 from Zhongshan to Dome A changed with the development of the event. The uppermost
375 site to detect the blocking is Dome A ~~with~~ at 4093 m a.s.l. and the average speed of the
376 blocking event across transect was about 40 km/h. Before 1st August, there was a drastic
377 drop in air pressure at AWSs from Zhongshan to Taishan, reaching the lowest value at
378 local noon, but the air pressure from Eagle to Dome A showed no such changes.
379 Meanwhile, the air temperature, relative humidity and wind speed show the opposite
380 change at all AWSs, rising sharply and reaching the highest values at local noon,
381 ~~average rose nearly 26%, 19% and 173% (compared with the time from 30th July to~~
382 ~~before the blocking event), respectively,~~ indicative of maritime air intrusions to the
383 PANDA transect. On 3 August, the deep low-pressure system was slightly weaker (not
384 shown). The southern section of the Indian Ocean subtropical high became ~~flat~~ weak in
385 the geopotential height anomaly field, and the blocking event moved eastward and
386 eventually dissipated d along the coast ~~or over the ocean surface~~. This event was similar
387 ~~to~~ like a recent abrupt warming event ~~in~~ at Dome C (Ding et al., 2022a). Therefore, the
388 PANDA AWS network provides high spatial-temporal observations and can play an
389 important role in ~~short-term weather forecast~~ the mesoscale circulation research on the
390 Antarctic Ice Sheet.

391 5. Data availability

392 This dataset is publicly available and it is planned that it will be updated on a near-
393 real time. The data from ~~the other all~~ AWSs will be publicly available on the A platform
394 “Big Earth Data Platform for Three Poles”; ~~the~~ The links are as follows: Zhongshan,
395 Panda 100, Panda 200, Panda 300, Panda 400, Taishan, Panda 1100 and Kunlun. t ~~The~~
396 data can be downloaded from <https://doi.org/10.11888/Atmos.tpd.272721> (Ding et al.,

2022b). Eagle and Dome A data has been published on the data portal of AAD: <http://aws.cdaso.cloud.edu.au/datapage.html>. Panda S data has been posted on the data portal of the University of Wisconsin: <https://doi.org/10.48567/1hn2-nw60> (AMRDC Data Repository).

6. Conclusion

In this paper, we have introduced the PANDA AWS network which can monitor the meteorology from the coastal Zhongshan AWS to ~~beyond~~ Panda S in the interior of the Antarctic continent with high spatial and temporal resolution. The data collected during the past decades are reliable after calibration and homogenization, and have been used widely in meteorological and climate change research in Antarctica (e.g., Xie et al., 2016, Ding et al. 2021a). The data can also be used to ~~derive surface energy balance,~~ assimilated into reanalyses, and used to evaluate climate models and to validate satellite data.

In a preliminary analysis, the diurnal, monthly, annual averages and as well as the long-term changes ~~of air temperature, relative humidity, air pressure, wind speed and direction~~ have been presented. They show distinctly significant differences between coastal, inland and dome summit regions. An example has also been given of a short-term atmospheric process to show this dataset's capability for weather monitoring and investigating.

Author contributions.

MD, IA and XZ designed the experiments and wrote the manuscript; MD carried out the experiments; XZ and DY analyzed the experimental results. MD, XZ, PH and DY revised the manuscript; CL, QS and WZ provides the information of AWS; DY, LB and CX discussed the results.

Competing interests.

The authors declare that they have no conflict of interest.

Acknowledgements.

The observations and AWS deployments were carried out during the Chinese National Antarctic Research Expedition from Zhongshan to Kunlun. We are grateful to David Mikolajczyk from Antarctic Meteorological Research and Data Center at the

427 University of Wisconsin for providing meteorological data and AWS information for
428 Panda S.

429 **Financial support.**

430 This research has been supported by the National Science Foundation of China
431 (42122047), the National Key Research and Development Program of China
432 (2021YFC2802504) and Basic fund of CAMS (2021Z006).

433

434 **Reference**

435 ~~Aristidi, E., Agabi, K., Azouit, M., Fossat, E., Vernin, J., Travouillon, T., Lawrence, J.~~
436 ~~S., Meyer, C., Storey, J. W. V., Halter, B., Roth, W. L., and Walden, V.: An analysis~~
437 ~~of temperatures and wind speeds above Dome C, Antarctica. *Astronomy &*~~
438 ~~*Astrophysics*, 430(2), 739-746, <https://doi.org/10.1051/0004-6361:20041876>, 2005.~~

439 Allison, I. and Morrissy, J.V.: Automatic weather stations in Antarctica. *Australian*
440 *Meteorological Magazine*, 31(2),71-76, 1983.

441 Allison, I., Wendler, G., and Radok, U.: Climatology of the East Antarctic ice sheet
442 (100°E to 140°E) derived from automatic weather stations, *Journal of Geophysical*
443 *Research: Atmospheres*, 98(D5), 8815-8823, <https://doi.org/10.1029/93JD00104>,
444 1993.

445 Allison, I. Surface climate of the interior of the Lambert Glacier basin, Antarctica, from
446 automatic weather station data. *Annals of Glaciology*, 27, 515-520.
447 <https://doi.org/10.3189/1998AoG27-1-515-520>, 1998.

448 Antarctic Meteorological Research and Data Center: Automatic Weather Station
449 quality-controlled observational data. AMRDC Data Repository. Subset used:
450 [DATE 1]-[DATE 2], accessed DD-MM-YYYY, [https://doi.org/10.48567/1hn2-](https://doi.org/10.48567/1hn2-nw60)
451 [nw60](https://doi.org/10.48567/1hn2-nw60).

452 Aristidi, E., Agabi, K., Azouit, M., Fossat, E., Vernin, J., Travouillon, T., Lawrence, J.
453 S., Meyer, C., Storey, J. W. V., Halter, B., Roth, W. L., and Walden, V.: An analysis
454 of temperatures and wind speeds above Dome C, Antarctica. *Astronomy &*
455 *Astrophysics*, 430(2), 739-746, <https://doi.org/10.1051/0004-6361:20041876>, 2005.

456

457 Bian, L., Allison, I., Xiao, C., Ma, Y., Fu, L., and Ding, M.: Climate and meteorological
458 processes of the East Antarctic ice sheet between Zhongshan and Dome-A, *Advances*
459 *in Polar Science*, 27(2), 90-101, <https://doi.org/10.13679/j.advps.2016.2.00090>,
460 2016.

461 Bromwich, D. H., Werner, K., Casati, B., Powers, J. G., Gorodetskaya, I. V., Massonnet,
462 F., Vitale, V., Heinrich, V. J., Liggett, D., Arndt, S., Barja, B., Bazile, E., Carpentier,
463 S., Carrasco, J. F., Choi, T., Choi, Y., Colwell, S. R., Cordero, R. R., Gervasi, M.,
464 Haiden, T., Hirasawa, Na., Inoue, J., Jung, T., Kalesse, H., Kim, S.J., Lazzara, M. A.,
465 Manning, K. W., Norris, K., Park, S. J., Reid P., Rigor, I., Rowe, P. M., Schmithüsen,
466 H., Seifert, P., Sun, Q., Uttal, T., Zannoni, M., and Zou, X.: The Year of Polar

467 Prediction in the Southern Hemisphere (YOPP-SH), *Bulletin of the American*
468 *Meteorological Society*, 101(10), E1653-E1676, [https://doi.org/10.1175/BAMS-D-](https://doi.org/10.1175/BAMS-D-19-0255.1)
469 [19-0255.1](https://doi.org/10.1175/BAMS-D-19-0255.1), 2020.

470 Chen, B., Zhang, R., Xiao, C., Bian, L., and Zhang, T.: Analyses on the air and snow
471 temperatures near ground with observations of an AWS at Dome A, the summit of
472 Antarctic Plateau, *Chinese Science Bulletin*, 55(11), 1048-1054,
473 <https://doi.org/10.1007/s11434-010-0099-1>, 2010.

474 ~~Clem, K.R., Fogt, R.L., Turner, J., Lintner B. R., Marshall G. J., Miller, J. R., and~~
475 ~~Renwick, J. A.: Record warming at the South Pole during the past three decades,~~
476 ~~*Nature Climate Chang.* 10, 762–770, <https://doi.org/10.1038/s41558-020-0815-z>,~~
477 ~~2020.~~

478 Das, I., Bell, R. E., Scambos, T. A., Wolovick, M., Creyts, T. T., Studinger, M., Frearson,
479 N., Nicolas, J. P., Lenaerts, J. T. M., and Van Den Broeke, M. R.: Influence of
480 persistent wind scour on the surface mass balance of Antarctica. *Nature Geoscience*,
481 6(5), 367-371 <https://doi.org/10.1038/ngeo1766>, 2013.

482 Ding, M., Xiao, C., Li, Y., Ren, J., Hou, S., Jin, B., and Sun, B.: Spatial variability of
483 surface mass balance along a traverse route from Zhongshan station to Dome A,
484 Antarctica, *Journal of Glaciology*, 57(204), 658-666,
485 <https://doi.org/10.3189/002214311797409820>, 2011.

486 Ding, M., Xiao, C., Li, C., Qin, D., Jin, B., Shi, G., Xie, A., and Cui, X.: Surface mass
487 balance and its climate significance from the coast to Dome A, East Antarctica,
488 *Science China Earth Sciences*, 58(10), 1787-1797, [https://doi.org/10.1007/s11430-](https://doi.org/10.1007/s11430-015-5083-9)
489 [015-5083-9](https://doi.org/10.1007/s11430-015-5083-9), 2015.

490 Ding, M., Yang, D., Van den Broeke, M. R., Allison, I., Xiao, C., Qin, D., and Huai, B.:
491 The surface energy balance at Panda 1 station, Princess Elizabeth Land: A typical
492 katabatic wind region in East Antarctica, *Journal of Geophysical Research:*
493 *Atmospheres*, 125(3), e2019JD030378, <https://doi.org/10.1029/2019JD030378>,
494 2020.

495 Ding, M., Zhang, T., Yang, D., Allison, I., Dou, T., and Xiao, C.: Brief communication:
496 Evaluation of multiple density-dependent empirical snow conductivity relationships
497 in East Antarctica, *Cryosphere*, 15, 4201-4206, [https://doi.org/10.5194/tc-15-4201-](https://doi.org/10.5194/tc-15-4201-2021)
498 [2021](https://doi.org/10.5194/tc-15-4201-2021), 2021a.

499 Ding, M., Du, F., Zhang, W., Wen, H., and Lu, C.: Battery system adapted to polar ultra-
500 low temperature environment and its temperature control method, Beijing:

501 CN113659246A, 2021b.

502 Ding, M., Xiao, C., and Qin, D.: Explosive warming event in Antarctica on 18 March
503 2022 and its possible causes. *Advances in Climate Change Research*,
504 <https://doi.org/10.12006/j.issn.1673-1719.2022.068>, 2022a.

505 Ding, M., Zou, X., Sun, Q., Yang, D., Zhang, W., Bian, L., Lu, C., Allison, I., Heil, P.,
506 and Xiao, C.: The PANDA automatic weather station network between the coast and
507 Dome A, East Antarctica (1989-2021). *A Big Earth Data Platform for Three Poles*,
508 <https://doi.org/10.11888/Atmos.tpc.272721>, 2022b.

509 Dong, X., Wang, Y., Hou, S., Ding, M., Yin, B., and Zhang, Y.: Robustness of the recent
510 global atmospheric reanalyses for Antarctic near-surface wind speed climatology,
511 *Journal of Climate*, 33(10), 4027-4043, <https://doi.org/10.1175/JCLI-D-19-0648.1>,
512 2020.

513 Enomoto, H., Warashina, H., Motoyama, H., Takahashi, S., and Koike, J.: Data-logging
514 automatic weather station along the traverse route from Syowa Station to Dome Fuji,
515 *Proc. of the NIPR Symp. on Polar Meteorol. and Glaciol.*, 9, 66-75,
516 <https://doi.org/10.15094/00003880>, 1995.

517 Heil, P.: Atmospheric conditions and fast ice at Davis, East Antarctica: A case study.
518 *Journal of Geophysical Research: Oceans*, 111(C5),
519 <https://doi.org/10.1029/2005JC002904>, 2006.

520 Hines, K. M., Bromwich, D. H., Wang, S. H., Silber, I., Verlinde, J., and Lubin, D.:
521 Microphysics of summer clouds in central West Antarctica simulated by the Polar
522 Weather Research and Forecasting model (WRF) and the Antarctic Mesoscale
523 Prediction System (AMPS), *Atmospheric Chemistry and Physics*, 19(19), 12431-
524 12454, <https://doi.org/10.5194/acp-19-12431-2019>, 2019.

525 Huai, B., Wang, Y., Ding, M., Zhang, J., and Dong, X.: An assessment of recent global
526 atmospheric reanalyses for Antarctic near surface air temperature, *Atmospheric
527 Research*, 226, 181-191, <https://doi.org/10.1016/j.atmosres.2019.04.029>, 2019.

528 Intergovernmental Panel on Climate Change.: IPCC special report on the ocean and
529 cryosphere in a changing climate, <https://archive.ipcc.ch/srocc/>, 2019.

530 King, J. C., Argentini, S. A., and Anderson, P. S.: Contrasts between the summertime
531 surface energy balance and boundary layer structure at Dome C and Halley stations,
532 Antarctica. *Journal of Geophysical Research: Atmospheres*, 111(D2),
533 <https://doi.org/10.1029/2005JD006130>, 2006.

534 Lazzara, M. A., Weidner, G. A., Keller, L. M., Thom, J. E., and Cassano, J. J.: Antarctic

535 automatic weather station program: 30 years of polar observation, Bulletin of the
536 American Meteorological Society, 93(10), 1519-1537, [https://doi.org/10.1175/B](https://doi.org/10.1175/BAMS-D-11-00015.1)
537 [AMS-D-11-00015.1](https://doi.org/10.1175/BAMS-D-11-00015.1), 2012.

538 Ma, Y., Bian, L., Xiao, C., Allison, I.: Correction of snow accumulation impacted on
539 air temperature from automatic weather station on the Antarctic Ice Sheet. Advance
540 in Polar Science, 20(04): 299-309, <http://ir.casnw.net/handle/362004/7877>, 2008.

541 Ma, Y., Bian, L., Xiao, C., Allison, I., and Zhou, X.: Near surface climate of the traverse
542 route from Zhongshan Station to Dome A, East Antarctica, Antarctic Science, 22(4),
543 443-459, <https://doi.org/10.1017/S0954102010000209>, 2010.

544 Ma, Y., and Bian, L.: A Surface Climatological Validation of ERA-interim Reanalysis
545 and NCEP FNL Analysis over East Antarctic, Chinese Journal of Polar Research,
546 26(4), 469-480, <https://doi.org/10.13679/j.jdyj.2014.4.469>, 2014.

547 Maturilli, M., Herber, A., and König-Langlo, G.: Climatology and time series of surface
548 meteorology in Ny-Ålesund, Svalbard, Earth System Science Data, 5(1), 155-163,
549 <https://doi.org/10.5194/essd-5-155-2013>, 2013.

550 Nigro, M. A., Cassano, J. J., and Seefeldt, M. W.: A weather-pattern-based approach to
551 evaluate the Antarctic Mesoscale Prediction System (AMPS) forecasts: Comparison
552 to automatic weather station observations, Weather and Forecasting, 26(2), 184-198,
553 <https://doi.org/10.1175/2010WAF2222444.1>, 2011.

554 Parish, T., and Bromwich, D.: The surface wind-field over the Antarctic ice sheets,
555 Nature 328, 51-54, <https://doi.org/10.1038/328051a0>, 1987.

556 Qin, D., and Ren, J.: The Antarctic Glaciology, Science Press, 2001.

557 Qin, T., Wei, L., and Ling, C.: The statistic and variance of cyclones enter in scientific
558 investigation station of China in Antarctic, Acta. Oceanologica Sinica, 39(5), 44-60,
559 <https://doi.org/10.3969/j.issn.0253-4193.2017.05.005>, 2017.

560 Radok, U., Allison, I. and Wendler, G.: Atmospheric surface pressure over the interior
561 of Antarctica. Antarctic Science, 8(2), 209-217, 1996.

562 Reijmer, C. H., and Oerlemans, J.: Temporal and spatial variability of the surface energy
563 balance in Dronning Maud Land, East Antarctica, Journal of Geophysical Research:
564 Atmospheres, 107(D24), ACL-9, <https://doi.org/10.1029/2000JD000110>, 2002.

565 Schwerdtfeger, W.: Weather and climate of the Antarctic, New York: Elsevier Science,
566 1984.

567 Smeets, P. C., Kuipers Munneke, P., Van As, D., van den Broeke, M. R., Boot, W.,
568 Oerlemans, H., Snellen, H., Reijmer, C.H., and van de Wal, R. S.: The K-transect in

569 west Greenland: Automatic weather station data (1993-2016), *Arctic, Antarctic, and*
570 *Alpine Research*, 50(1), S100002, <https://doi.org/10.1080/15230430.2017.1420954>,
571 2018.

572 Sun, Q. Z., Zhang, L., Meng, S., Shen, H., Ding, Z. M., and Zhang, Z. H.:
573 Meteorological observations and weather forecasting services of the CHINARE, *Adv*
574 *Polar Sci*, 28 (4), 291-299, <https://doi.org/10.13679/j.advps.2018.4.00291>, 2018.

575 Turner, J., Colwell, S. R., Marshall, G. J., Lachlan-Cope, T. A., Carleton, A. M., Jones,
576 P. D., Lagun V., Reid P. A., and Iagovkina, S.: Antarctic climate change during the
577 last 50 years, *International Journal of Climatology*, 25(3), 279-294,
578 <https://doi.org/10.1002/joc.1130>, 2005.

579 Turner, J., Overland, J. E., and Walsh, J. E.: An Arctic and Antarctic perspective on
580 recent climate change, *International Journal of Climatology: A Journal of the Royal*
581 *Meteorological Society*, 27(3), 277-293, <https://doi.org/10.1002/joc.1406>, 2007.

582 Turner, J., Marshall, G. J., Clem, K., Colwell, S., Phillips, T., and Lu, H.: Antarctic
583 temperature variability and change from station data. *International Journal of*
584 *Climatology*, 40(6), 2986-3007, <https://doi.org/10.1002/joc.6378>, 2020.

585 Van As, D., Van den Broeke, M. R., and Van De Wal, R.: Daily cycle of the surface
586 layer and energy balance on the high Antarctic Plateau, *Antarctic Science*, 17(1), 121-
587 133, <https://doi.org/10.1017/S095410200500252X>, 2005.

588 Van den Broeke, M. R., Van Lipzig, N. P. M., and Van Meijgaard, E.: Momentum budget
589 of the East Antarctic atmospheric boundary layer: Results of a regional climate model,
590 *Journal of the Atmospheric Sciences*, 59(21), 3117-3129,
591 [https://doi.org/10.1175/1520-0469\(2002\)059<3117:MBOTEA>2.0.CO;2](https://doi.org/10.1175/1520-0469(2002)059<3117:MBOTEA>2.0.CO;2), 2002.

592 Van den Broeke, M. R., and Van Lipzig, N. P. M.: Factors controlling the near-surface
593 wind field in Antarctica, *Monthly Weather Review*, 131(4), 733-743,
594 [https://doi.org/10.1175/1520-0493\(2003\)131<0733:FCTNSW>2.0.CO;2](https://doi.org/10.1175/1520-0493(2003)131<0733:FCTNSW>2.0.CO;2), 2003.

595 Van den Broeke, M. R., Reijmer, C. H., and Van De Wal, R.: Surface radiation balance
596 in Antarctica as measured with automatic weather stations, *Journal of Geophysical*
597 *Research: Atmospheres*, 109(D9), <https://doi.org/10.1029/2003JD004394>, 2004a.

598 Van den Broeke, M. R., Reijmer, C. H., and Van De Wal, R. S.: A study of the surface
599 mass balance in Dronning Maud Land, Antarctica, using automatic weather stations,
600 *Journal of Glaciology*, 50(171), 565-582,
601 <https://doi.org/10.3189/172756504781829756>, 2004b.

602 Van den Broeke, M. R., Reijmer, C. H., Van As, D., Van de Wal, R., and Oerlemans, J.:

603 Seasonal cycles of Antarctic surface energy balance from automatic weather stations,
604 *Annals of Glaciology*, 41, 131-139, <https://doi.org/10.3189/172756405781813168>,
605 2005.

606 Van Den Broeke, M. R., Reijmer, C. H., Van As, D., and Boot, W.: Daily cycle of the
607 surface energy balance in Antarctica and the influence of clouds, *International*
608 *Journal of Climatology: A Journal of the Royal Meteorological Society*, 26(12),
609 1587-1605, <https://doi.org/10.1002/joc.1323>, 2006.

610 Vignon, E., Genthon, C., Barral, H., Amory, C., Picard, G., Gallée, H., Casasanta, G.,
611 and Argentini, S.: Momentum-and heat-flux parametrization at Dome C, Antarctica:
612 A sensitivity study, *Boundary-Layer Meteorology*, 162(2), 341-367,
613 <https://doi.org/10.1007/s10546-016-0192-3>, 2017.

614 Wang, S., Ding, M., Liu, G., Wei, T., Zhang, W., Chen, W., Dou, T., and Xiao, C.: On
615 the Drivers of Temperature Extremes on the Antarctic Peninsula During Austral
616 Summer, *Climate Dynamics*, <https://doi.org/10.1007/s00382-022-06209-0>, 2022.

617 Wawrzyniak, T., and Osuch, M.: A 40-year High Arctic climatological dataset of the
618 Polish Polar Station Hornsund (SW Spitsbergen, Svalbard), *Earth System Science*
619 *Data*, 12(2), 805-815, <https://doi.org/10.5194/essd-12-805-2020>, 2020.

620 Wei, T., Yan, Q., and Ding, M.: Distribution and temporal trends of temperature
621 extremes over Antarctica, *Environmental Research Letters*, 14(8), 084040,
622 <https://doi.org/10.1088/1748-9326/ab33c1>, 2019.

623 Wendler, G., Ishikawa, N., and Kodama, Y.: The heat balance of the Icy slope of Adelie
624 Land, Eastern Antarctica, *Journal of Applied Meteorology*, 27(1), 52-65,
625 [https://doi.org/10.1175/1520-0450\(1988\)027<0052:THBOTI>2.0.CO;2](https://doi.org/10.1175/1520-0450(1988)027<0052:THBOTI>2.0.CO;2), 1988.

626 Xiao, C., Li, Y., Allison, I., Hou, S., Dreyfus, G., Barnola, J. M., Ren, J., Bian, L., Zhang,
627 S., and Kameda, T.: Surface characteristics at Dome A, Antarctica: first
628 measurements and a guide to future ice-coring sites, *Annals of Glaciology*, 48, 82-
629 87, <https://doi.org/10.3189/172756408784700653>, 2008.

630 Xie, A., Allison, I., Xiao, C., Wang, S., Ren, J., and Qin, D.: Assessment of surface
631 pressure between Zhongshan and Dome A in East Antarctica from different
632 meteorological reanalyses. *Arctic, Antarctic, and Alpine Research*, 46(3), 669-681,
633 <https://doi.org/10.1657/1938-4246-46.3.669>, 2014.

634 Xie, A., Wang, S., Xiao, C., Kang, S., Gong, J., Ding, M., Li, C., Dou, T., Ren, J., and
635 Qin, D.: Can temperature extremes in East Antarctica be replicated from ERA Interim
636 reanalysis? *Arctic, Antarctic, and Alpine Research*, 48(4), 603-621,

637 <https://doi.org/10.1657/AAAR0015-048>, 2016.

638 [Zeng, Z., Wang, Z., Ding, M., Zheng, X., Sun, X., Zhu, W., Zhu, K., An, J., Zang, L.,](#)
639 [Guo, J., and Zhang, B.: Estimation and Long-term Trend Analysis of Surface Solar](#)
640 [Radiation in Antarctica: A Case Study of Zhongshan Station. Advances in](#)
641 [Atmospheric Sciences, 38\(9\), 1497-1509, https://doi.org/10.1007/s00376-021-0386-](#)
642 [6, 2021.](#)

643 Zhang, S., E, D., Wang, Z., Li, Y., Jin, B., and Zhou, C.: Ice velocity from static GPS
644 observations along the transect from Zhongshan station to Dome A, East Antarctica,
645 Annals of Glaciology, 48, 113-118, <https://doi.org/10.3189/172756408784700716>,
646 2008.

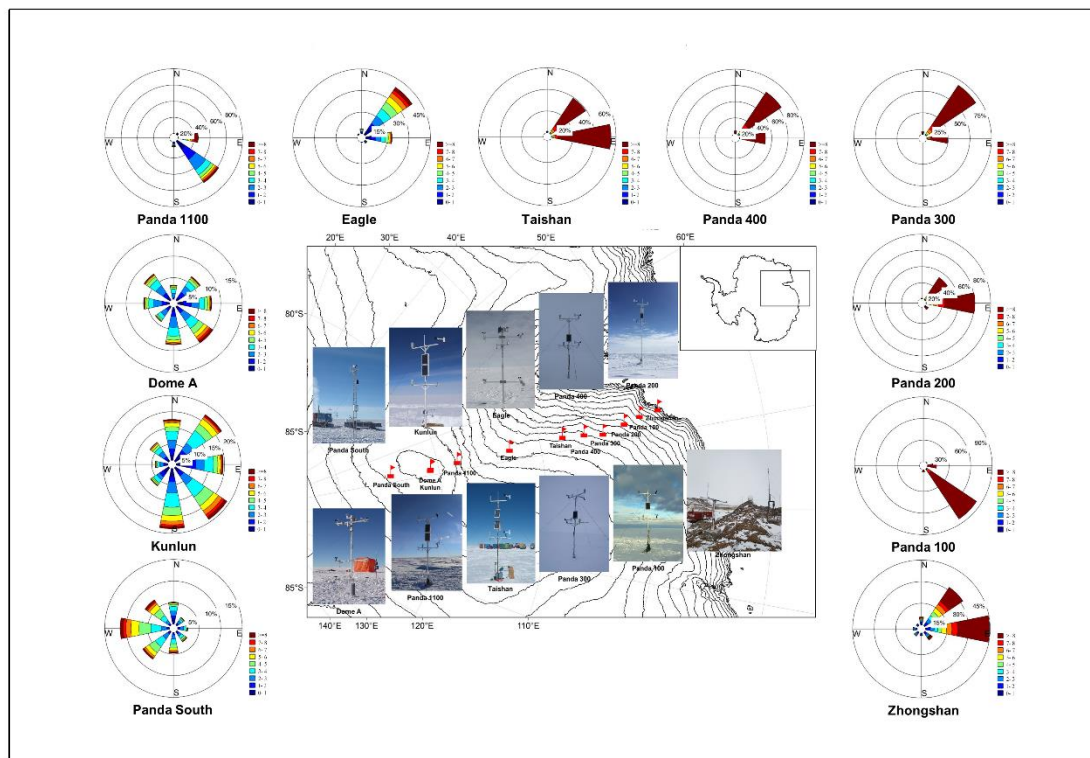
647 Zhang, Y., Wang, Y., and Hou, S.: Reliability of Antarctic air temperature changes from
648 Polar WRF: A comparison with observations and MAR outputs, Atmospheric
649 Research, 105967, <https://doi.org/10.1016/j.atmosres.2021.105967>, 2021.

650 Zhou, M., Zhang, Z., Zhong, S., Lenschow, D., Hsu, H. M., Sun, B., Gao, Z., Li, S.,
651 Bian, X., and Yu, L.: Observations of near-surface wind and temperature structures
652 and their variations with topography and latitude in East Antarctica, Journal of
653 Geophysical Research: Atmospheres, 114(D17),
654 <https://doi.org/10.1029/2008JD011611>, 2009.

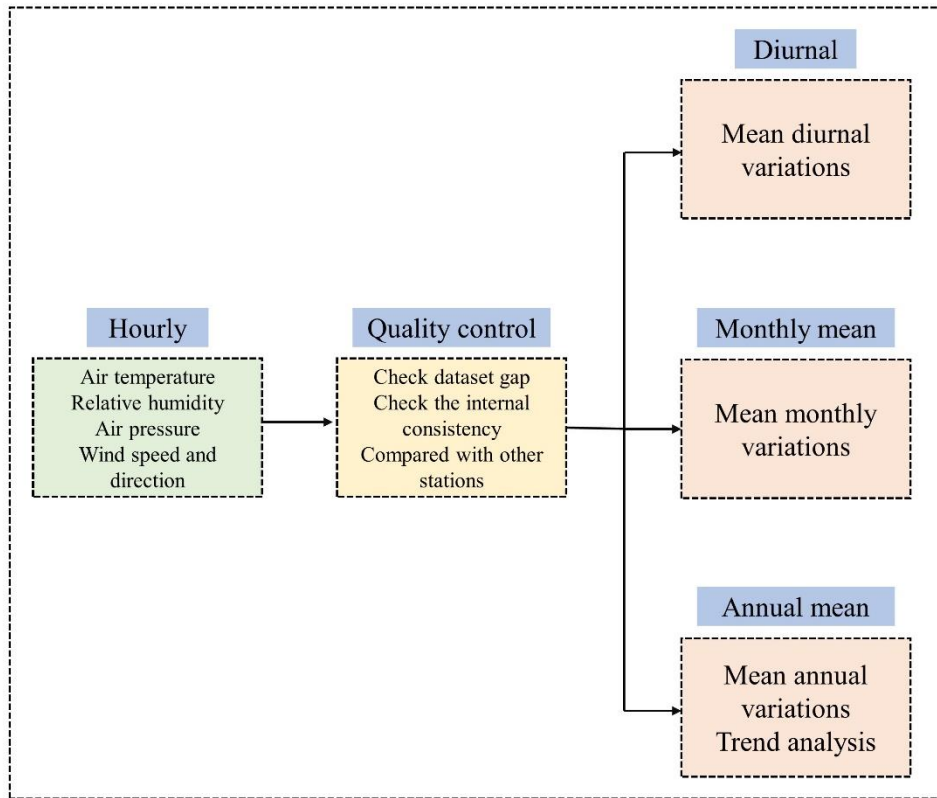
655 Zou, X., Ding, M., Sun, W., Yang, D., Liu, W., Huai, B., Jin, S., and Xiao, C.: The
656 surface energy balance of Austre Lovénbreen, Svalbard, during the ablation period
657 in 2014, Polar Research, 40, <https://doi.org/10.33265/polar.v40.5318>, 2021.

658

659 **Figures and Table:**

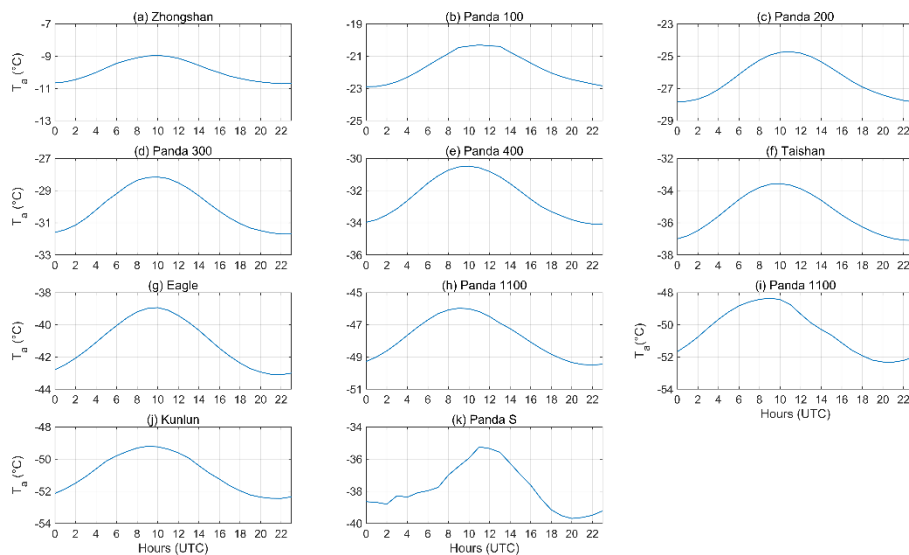


660
 661 Figure 1. The location and Wind roses of AWSs in the PANDA network. The red flags
 662 are AWSs; the black solid lines are 200_m interval contours. The wind directions are
 663 divided into 22.5° sectors. Zhongshan is calculated during 1989-2020; Panda 100,
 664 Panda 300 and Panda 400 are calculated during 2019-2021; Panda 200 is calculated
 665 during 2016-2021; Taishan is calculated during 2012-2021; Eagle and Dome A are
 666 calculated during 2005-2020; Kunlun is calculated during 2017-2021; and Panda S
 667 is calculated during 2008-2021. Note however that, because some winter data were
 668 unreliable, Eagle averages exclude Mar-Aug; Dome A averages exclude March-
 669 October; and Panda S averages exclude May-September.
 670



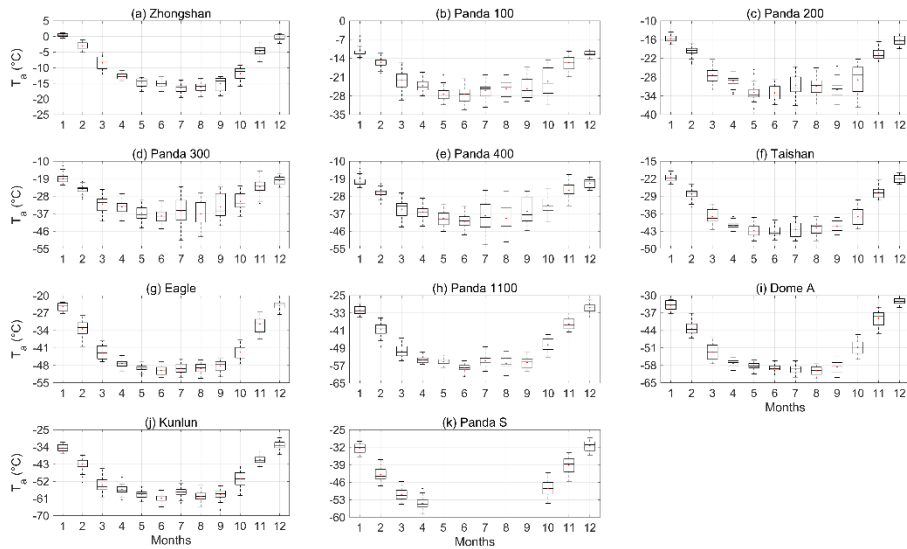
671
672
673
674

Figure 2. Schematic diagram of data processing workflow used to compile the AWS meteorology dataset for the network.



675
676
677
678
679

Figure 3. Average diurnal variation of air temperature at AWSs in the PANDA network. The calculation years for these sites are the same as in Fig. 1, excepting that Zhongshan is calculated during 2002-2020.



680

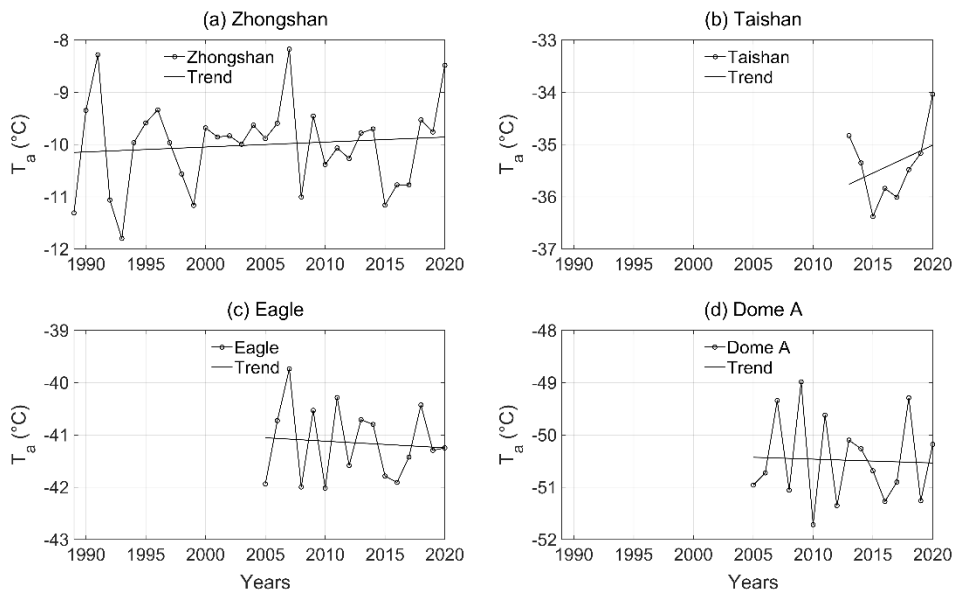
681 Figure 4. Variation of monthly mean air temperature at AWSs in the PANDA network.

682 The calculation periods for these sites are the same as [in-for](#) Fig. 3, For each monthly

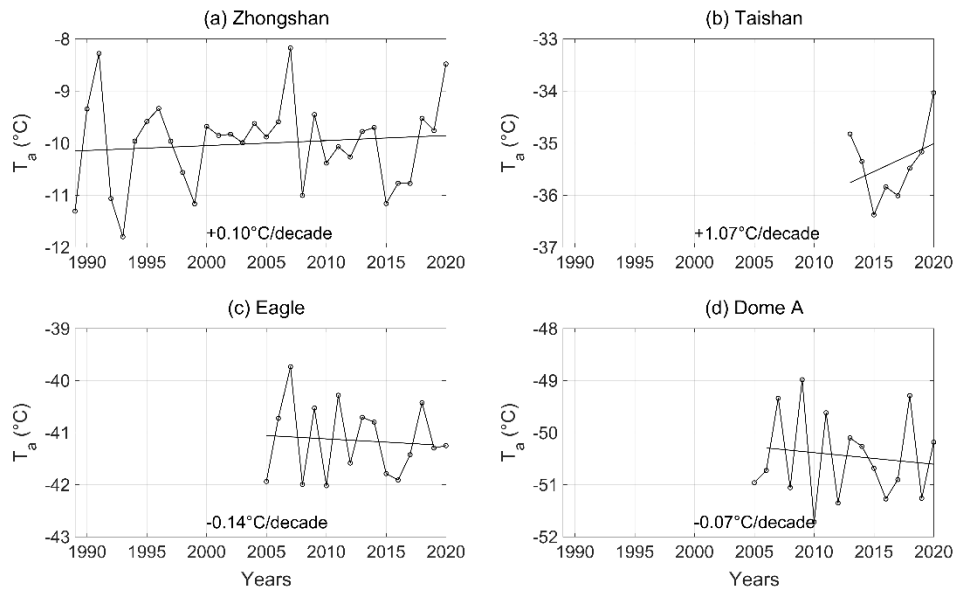
683 box, the central line indicates the median, the red dot represents the mean, and the

684 bottom and top edges of the box indicate the 25th and 75th percentiles, respectively.

685



686



687

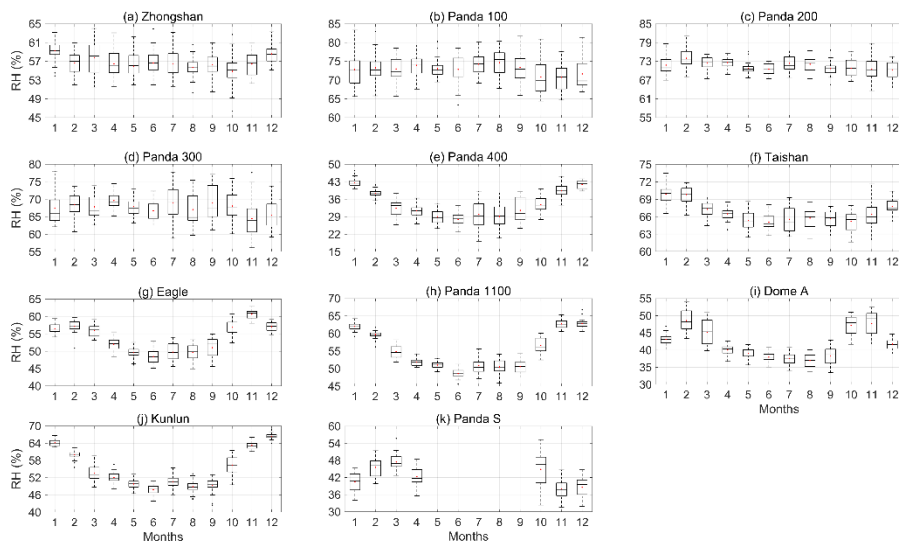
688

689

690

691

Figure 5. Interannual variation of~~Variation of annual mean~~ air temperature at Zhongshan, Taishan ($P<0.05$), Eagle and Dome A. Zhongshan is calculated during 1989-2020; Taishan is calculated during 2013-2020; Eagle and Dome A are calculated during 2005-2020.



692

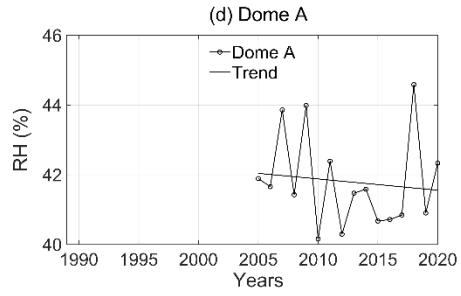
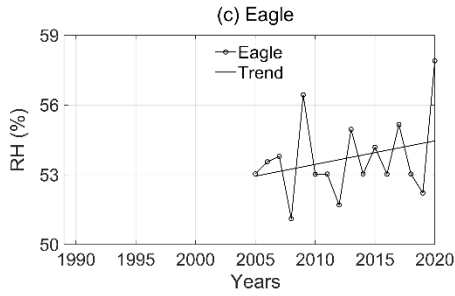
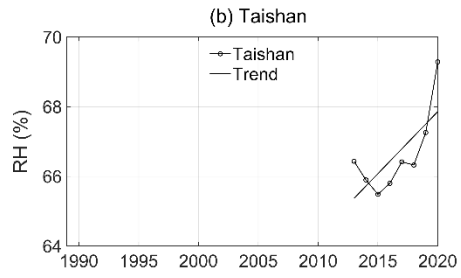
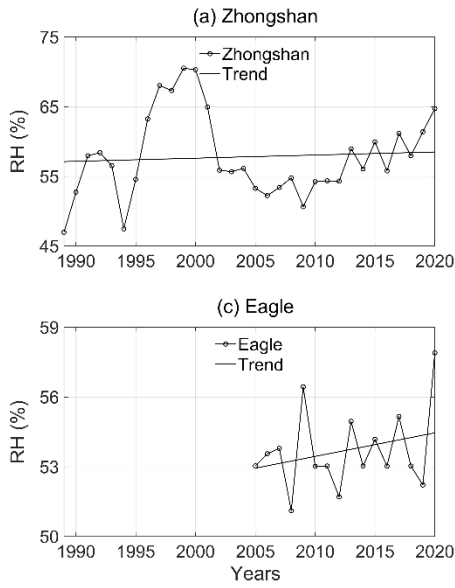
693

694

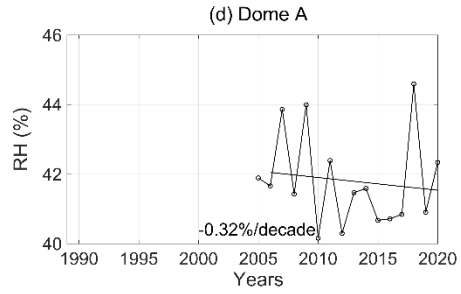
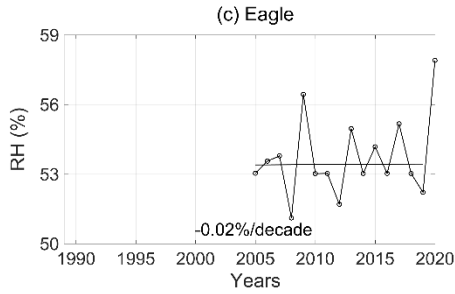
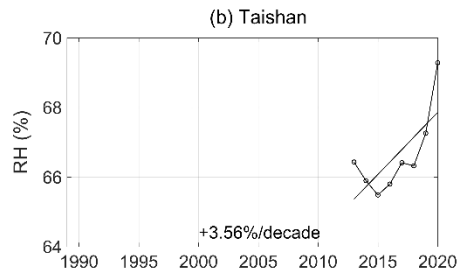
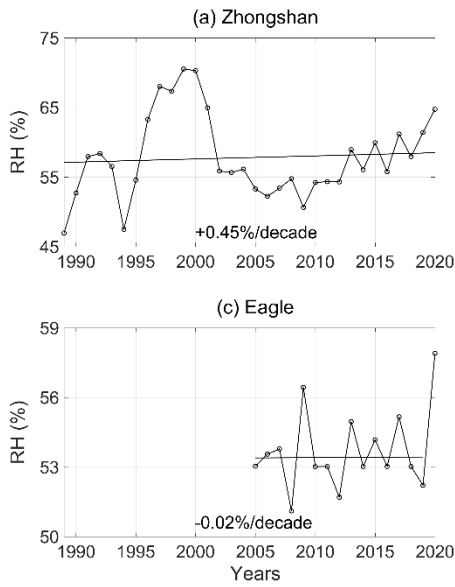
695

Figure 6. Monthly variation of relative humidity at AWSs in the PANDA network.

The calculation periods of these sites are the same as [in-for](#) Fig. 3.



696

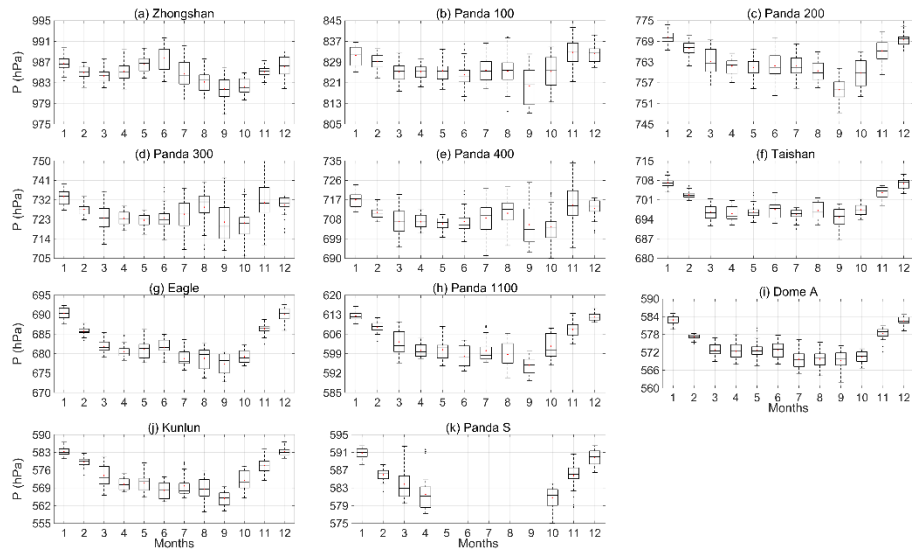


697

698

699

Figure 7. Interannual-Annual variation of relatively humidity at Zhongshan ($p<0.05$), Taishan ($p<0.05$), Eagle and Dome A.

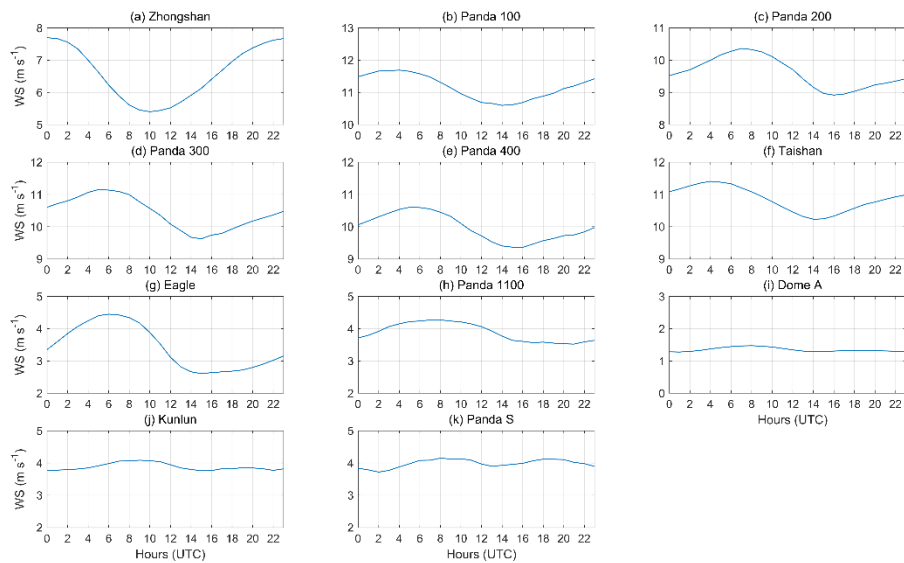


700

701

702

Figure 8. Monthly variation of air pressure at AWSs in the PANDA network. The calculation periods at these sites are the same as [in-for](#) Fig. 3.



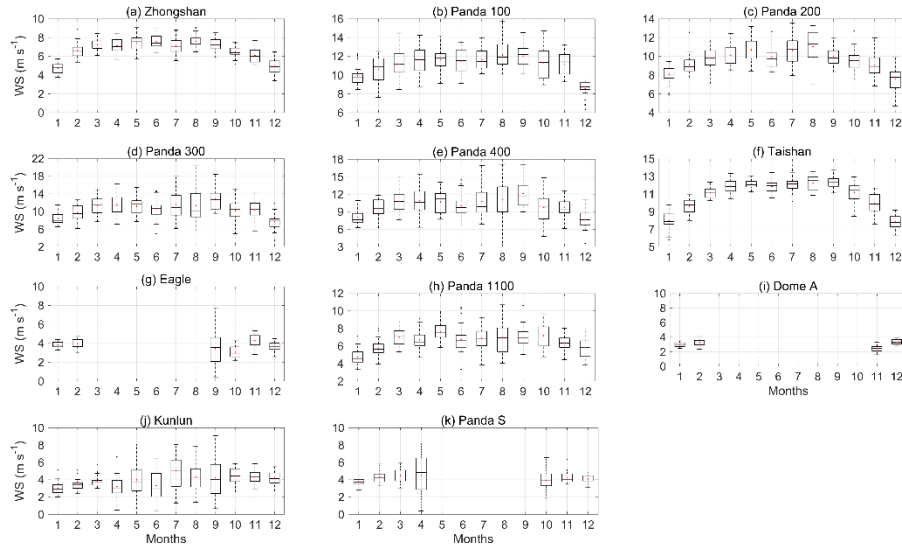
703

704

705

706

Figure 9. Diurnal variation of wind speed of PANDA AWSs network. The calculation periods of these site are the same [with-as for](#) Fig. 1, Zhongshan is calculated during 2002-2020.

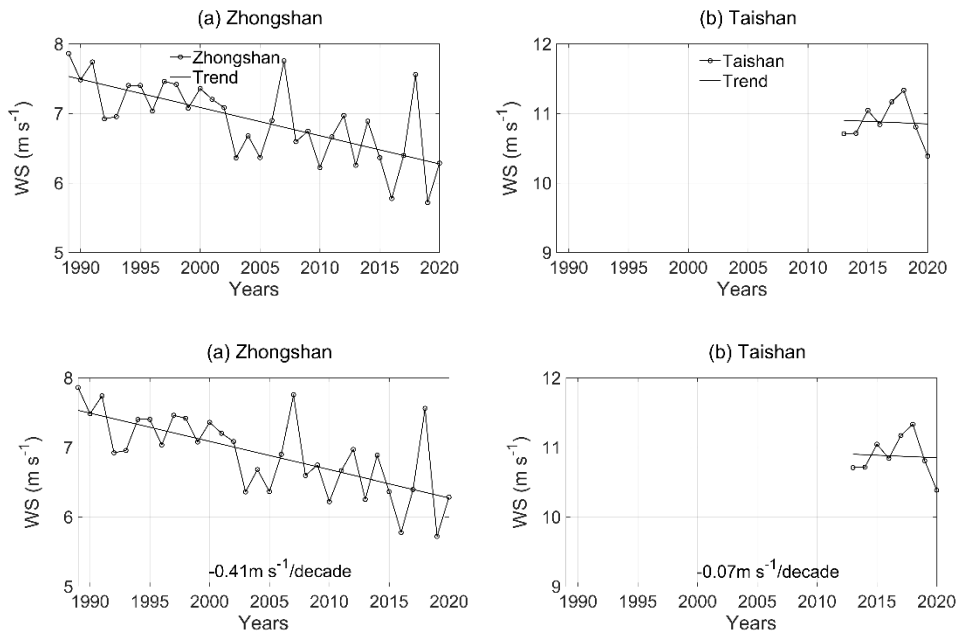


707

708

Figure 10. Monthly variation of wind speed of PANDA AWSs network. The calculation periods of these sites are the same [with-as for Fig. 1](#).

709



710

711

712

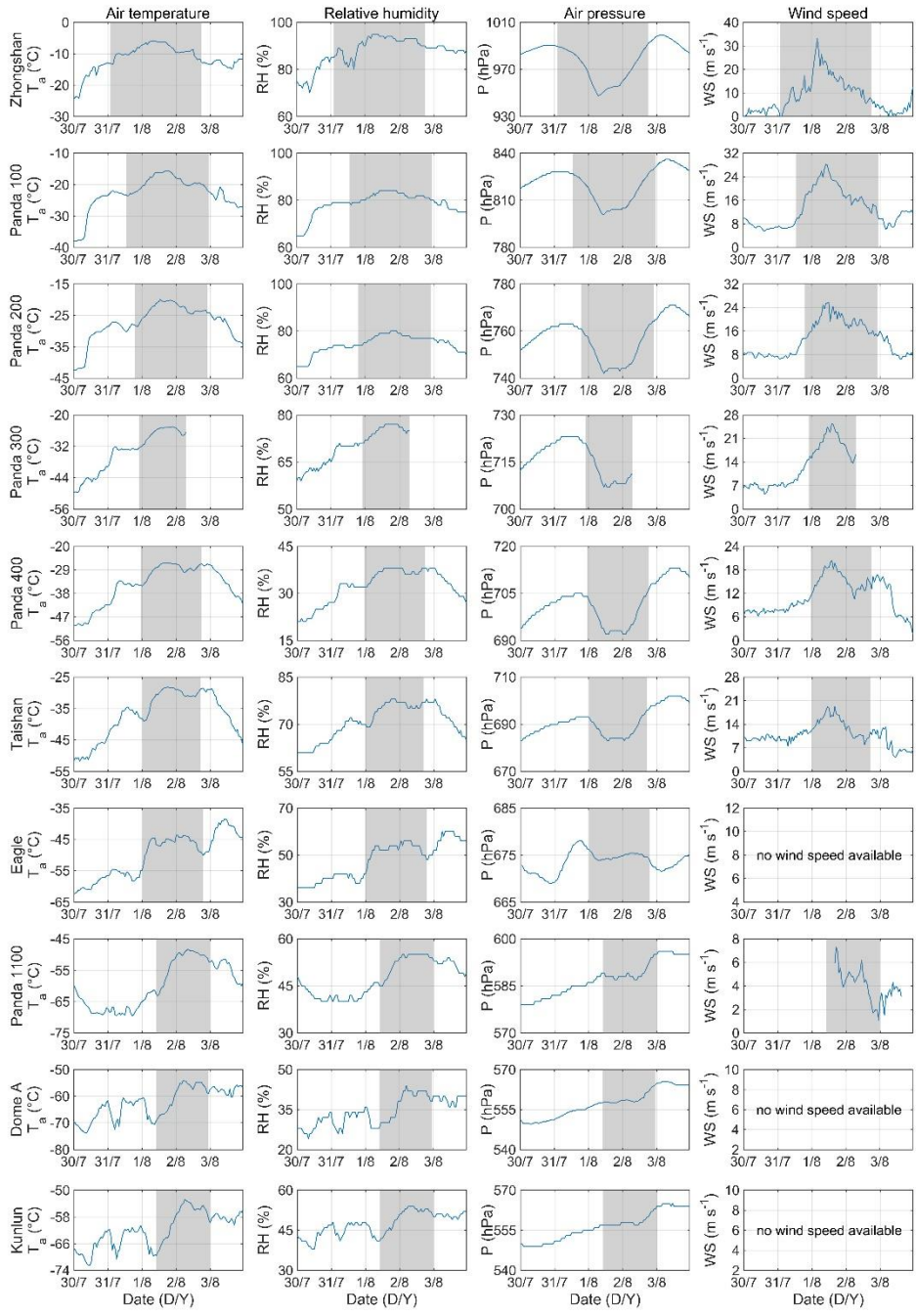
Figure 11. Annual variation of wind speed at Zhongshan ($P < 0.05$) and Taishan ($P < 0.05$). The calculation periods of these site are the same [with-as for Fig. 5](#).

713

714

715

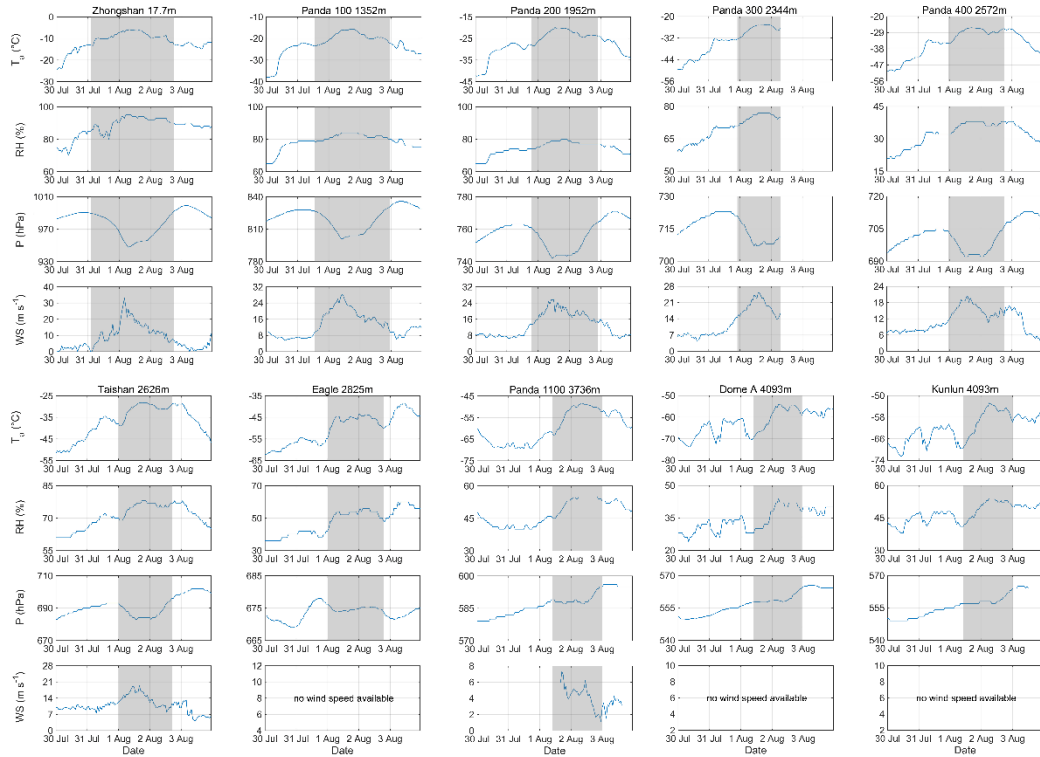
716



717

718

719



720

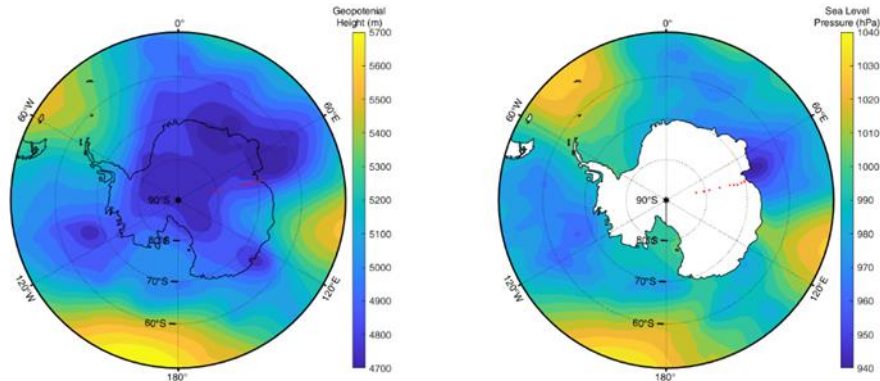
721

722

723

724

Figure 12. Time series of Changes in air temperature, relative humidity, air pressure and wind speed at AWS of the PANDA network (except Panda S) from 00:00 30th July to 23:00 3rd August 2020 (UTC); gray zone: blocking event.



725

726

727

Figure 13. The mean 500 hPa geopotential height (left) and sea level pressure (right) on 12:00 1st August (red dot: surface weather station).

728
729

Table 1. Locations, operational periods, observed variables and heights, and instrumentation and accuracies of AWSs in the PANDA network

Stations	Location	Altitude	Period(Y/M)	Variable	Sensor	Accuracy	Height
Zhongshan	69.37°S 76.38°E	17.7 m a.s.l.	1989/03- 2020/12	Ta/RH	<u>Vaisala</u> HMP155	(0.2260- 0028*Ta) °C/1%	2m
				P	<u>Campbell</u> CS106	1.5hPa	2m
				WS/WD	<u>Huayun</u> XFY3-1	1m s ⁻¹ /5°	10m
Panda 100	70.22°S 76.65°E	1352 m a.s.l.	2019/02- 2021/07	Ta/RH	<u>Vaisala</u> HMP155	(0.2260- 0028*Ta) °C/1%	2/4m
				P	<u>Vaisala</u> PTB110	0.3hPa	2m
				WS/WD	<u>Huayun</u> XFY3-1	1m s ⁻¹ /5°	2/4m
				SDR/SUR	Li200X	5% Max/3% Typical	2m
Panda 200	70.97°S 77.19°E	1952 m a.s.l.	2016/12- 2021/07	Ta/RH	<u>Vaisala</u> HMP155	(0.2260- 0028*Ta) °C/1%	4/6m
				P	<u>Vaisala</u> PTB210	0.5hPa	4m
				WS/WD	<u>Huayun</u> XFY3-1	1m s ⁻¹ /5°	4/6m
				SDR/SUR	Li200X	5% Max/3% Typical	4m
Panda 300	72.00°S 77.95°E	2344 m a.s.l.	2019/12- 2021/07	Ta/RH	<u>Vaisala</u> HMP155	(0.2260- 0028*Ta) °C/1%	2/4m
				P	<u>Vaisala</u> PTB210	0.5hPa	2/4m
				WS/WD	<u>Huayun</u> XFY3-1	1m s ⁻¹ /5°	2/4m
				SDR/SUR	Li200X	5% Max/3% Typical	2m
Panda 400	72.86°S 77.38°E	2572 m a.s.l.	2019/12- 2021/07	Ta/RH	<u>Vaisala</u> HMP155	(0.2260- 0028*Ta) °C/1%	1/2/4m
				P	<u>Vaisala</u> PTB210	0.5hPa	2m
				WS/WD	<u>Huayun</u> XFY3-1	1m s ⁻¹ /5°	1/2/4m
				SDR/SUR/LDR/LUR	Li200X	5% Max/3% Typical	2m
Taishan	73.86°S 76.98°E	2626 m a.s.l.	2012/12- 2021/07	Ta/RH	<u>Vaisala</u> HMP155	(0.2260- 0028*Ta) °C/1%	2/4m
				P	<u>Vaisala</u> PTB110	0.3hPa	2m
				WS/WD	<u>Huayun</u> XFY3-1	1m s ⁻¹ /5°	2/4m
				SDR/SUR	CNR4	10%	2m
Eagle	76.42°S 77.02°E	2825 m a.s.l.	2005/01- 2020/12	Ta	FS23D		
				RH	<u>Vaisala</u> HMP35D	0.05°C	1/2/4m
				P	<u>Paroscientific</u>	2%	2m
				WS/WD	6015A	0.5hPa	2m
				Ta	<u>RM Young</u> 12170C/ <u>Aanderaa</u> 3590B	0.5m s ⁻¹ /6°	1/2/4m

					RH			
					P			
					WS/WD			
Panda 1100	79.01°S 76.99°E	3736 m a.s.l.	2019/01- 2021/07		Ta/RH	<u>Vaisala</u> HMP155	(0.2260- 0028*Ta) °C/1%	2/4m
					P	<u>Vaisala</u> PTB210	0.5hPa	2m
					WS/WD	<u>Huayun</u> XFY3-1	1m s ⁻¹ /5°	2/4m
					SDR/SUR	Li200X	5% Max/3% Typical	2/4m
Dome A	80.37°S 77.37°E	4093 m a.s.l.	2005/01- 2020/12		Ta			
					RH	FS23D		
					P	<u>Vaisala</u> HMP35D	0.05°C	1/2/4m
						<u>Paroscientific</u>	2%	4m
					WS/WD	6015A	0.5hPa	2m
					Ta	<u>RM Young</u>		
					RH	12170C/	0.5m s ⁻¹ /6°	1/2/4m
	P	<u>Aanderaa</u> 3590B						
				WS/WD				
Kunlun	80.43°S 77.12°E	4093 m a.s.l.	2017/01- 2021/07		Ta	Campbell_109/ <u>Vaisala</u> HMP155	(0.2260- 0028*Ta) °C/1%	2/4m
					RH	<u>Vaisala</u> HMP155	(0.2260- 0028*Ta) °C/1%	4m
					P	<u>Vaisala</u> PTB210	0.5hPa	2m
					WS/WD	<u>Huayun</u> XFY3-1	1m s ⁻¹ /5°	4m
					SDR/SUR	Li200X	5% Max/3% Typical	2m
Panda S	82.33°S 75.99°E	4027 m a.s.l.	2008/01- 2021/04		Ta	PRT 2-wire Bridge	0.5°C	4m
					RH	<u>Vaisala</u> HMP35A	5%	4m
					P	<u>Paroscientific</u> Model-215 A	0.2hPa	4m
					WS/WD	RM_Young/10K Ohmpot	0.2±0.5m s ⁻¹ /3°	4m

730 ~~Statement: SDR: downward shortwave radiation; SUR: upward shortwave radiation;~~
731 ~~LDR: downward longwave radiation; LUR: upward longwave radiation.~~
732

733

734

Table 2 The mean values of meteorological variables on AWSs in the PANDA

735

network

736

737

738

739

740

741

742

743

744

745

746

747

748

749

750

751

752

Stations\ elements	Air temperature /°C	Relative humidity/%	Pressure /hPa	Wind speed /m s ⁻¹	<u>Number of hourly values</u> [IA1]
Zhongshan	-10.0	58	985	6.9	<u>184695</u>
Panda 100	-21.6	73	827	11.2	<u>21216</u>
Panda 200	-26.5	72	763	10.9	<u>40010</u>
Panda 300	-30.0	68	726	10.4	<u>13811</u>
Panda 400	-32.0	34	710	10.0	<u>13783</u>
Taishan	-35.4	67	699	10.9	<u>74893</u>
Eagle	-41.2	54	683	3.6	<u>139608</u>
Panda 1100	-47.7	55	603	3.6	<u>39648</u>
Dome A	-50.5	42	575	2.9	<u>140484</u>
Kunlun	-50.8	55	574	3.9	<u>39515</u>
Panda S	<u>-39.2</u>	<u>-42</u>	<u>-587</u>	<u>-4.0</u>	<u>=</u>